Biochemistry

© Copyright 2003 by the American Chemical Society Volume 42, Number 24 June 24, 2003

Current Topics

Biochemistry and Structural DNA Nanotechnology: An Evolving Symbiotic Relationship†

Nadrian C. Seeman*

Department of Chemistry, New York University, New York, New York 10003, USA

Received March 31, 2003

ABSTRACT: Structural DNA nanotechnology is derived from naturally occurring structures and phenomena in cellular biochemistry. Motifs based on branched DNA molecules are linked together by sticky ends to produce objects, periodic arrays, and nanomechanical devices. The motifs include Holliday junction analogues, double and triple crossover molecules, knots, and parallelograms. Polyhedral catenanes, such as a cube or a truncated octahedron, have been assembled from branched junctions. Stiff motifs have been used to produce periodic arrays, containing topographic features visible in atomic force microscopy; these include deliberately striped patterns and cavities whose sizes can be tuned by design. Deliberately knotted molecules have been assembled. Aperiodic arrangements of DNA tiles can be used to produce assemblies corresponding to logical computation. Both DNA structural transitions and branch migration have been used as the basis for the operation of DNA nanomechanical devices. Structural DNA nanotechnology has been used in a number of applications in biochemistry. An RNA knot has been used to establish the existence of RNA topoisomerase activity. The sequence dependence of crossover isomerization and branch migration at symmetric sites has been established through the use of symmetric immobile junctions. DNA parallelogram arrays have been used to determine the interhelical angles for a variety of DNA branched junctions. The relationship between biochemistry and structural DNA nanotechnology continues to grow.

Biochemistry is a nanoscale phenomenon. Most of the macromolecular components of the cell, such as proteins or RNA, nucleosomes or ribosomes, have dimensions on the order of a few nanometers; larger constructs, such as microtubules or microfilaments, have components on this scale. The DNA double helix itself is inherently a nanoscale object; its diameter is about 20 Å (2 nm) and the separation of the bases is 3.4 Å; the helical periodicity is 10−10.5 nucleotide pairs per turn, or ∼3.5 nm per turn. It seems natural that the structural and biochemical knowledge of DNA gained over the past 50 years should be used in the emerging field nanotechnology. The purpose of this article is to describe the state of the art in structural DNA nanotechnology, and to demonstrate how the field has developed from biochemical systems and methods. There are now a few instances where structural DNA nanotechnology has been used to make biochemical measurements and to establish principles; these applications, as well as projected biochemical applications also will be discussed.

† This research has been supported by Grants GM-29554 from the National Institute of General Medical Sciences, N00014-98-1-0093 from the Office of Naval Research, Grants DMI-0210844, EIA-0086015, DMR-01138790, and CTS-0103002 from the National Science Foundation, and F30602-01-2-0561 from DARPA/AFSOR.

* E-mail: ned.seeman@nyu.edu. Phone: 212-998-8395. FAX: 212-260-7905.

10.1021/bi030079v CCC: $25.00 © 2003 American Chemical Society
Published on Web 05/24/2003

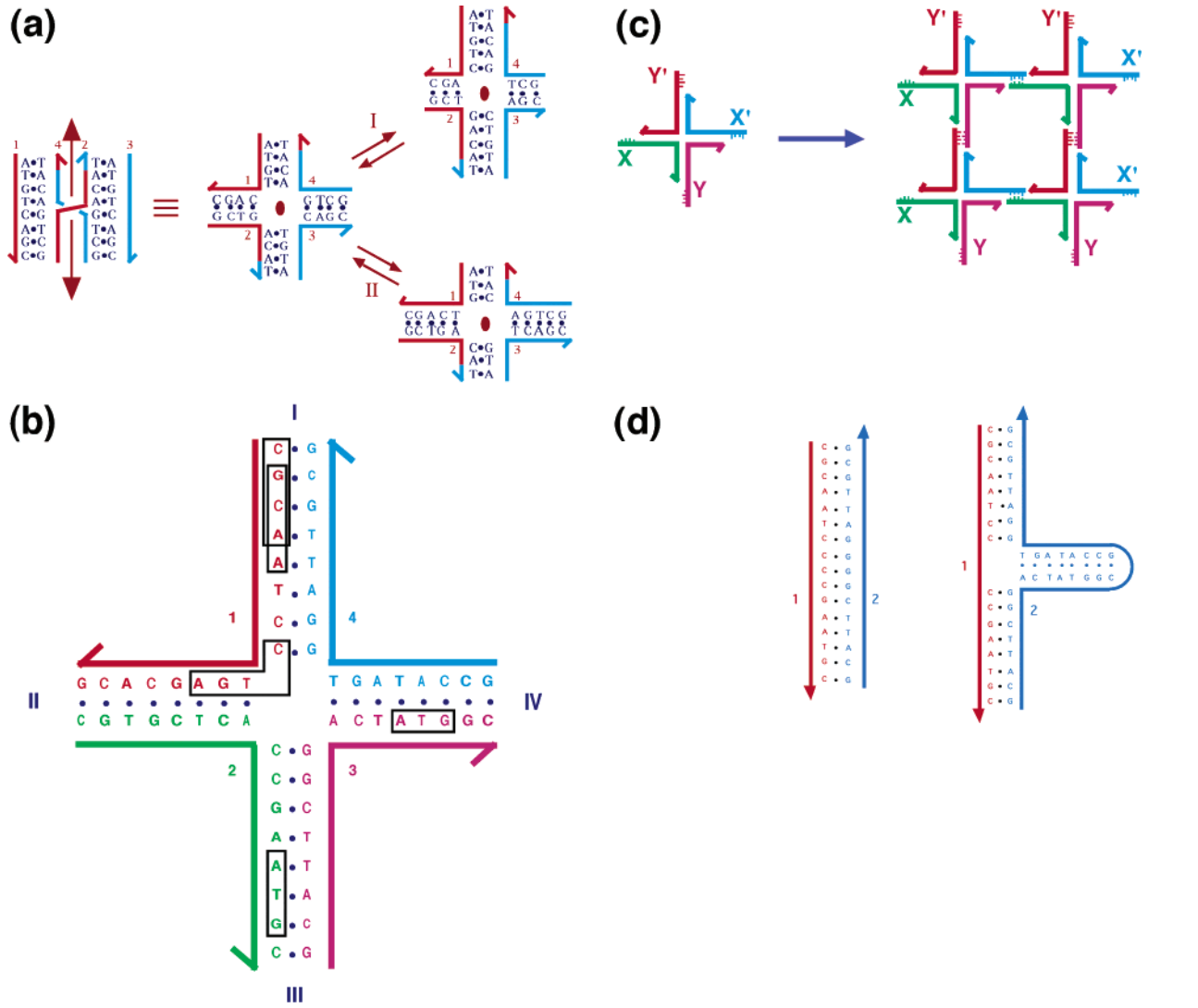

FIGURE 1: Branched Molecules. (a) Branch migration. On the left, two homologous duplexes, red and blue, have undergone reciprocal exchange. There is a vertical dyad axis of sequence symmetry. In the center, the drawing has been rearranged so that the dyad is perpendicular to the page. Through the isomerization process of branch migration, the C's and G's flanking the junction exchange partners (process I), or the A's and T's exchange partners (process II). (b) A stable branched junction. There is no dyad symmetry flanking the branch point; tetramers, such as the boxed sequences CGCA and GCAA are unique, and there is no TCAG to complement the CTGA flanking the corner. (c) Self-assembly of branched junctions. A stable branched junction with sticky ends X and X′, Y and Y′ are seen to form a quadrilateral. The sticky ends on the outside of the quadrilateral could be used to form a 2D array. (d) Inexact complementarity in branched DNA. On the left is a DNA duplex, and on the right is a three-arm branched junction. The strands of both molecules are labeled 1 and 2; both strands 1 are identical. Every nucleotide of strand 1 on the right is complemented by a nucleotide in strand 2, but there are many nucleotides in the branch whose sequences are irrelevant to the complementarity between strands 2 and 1.

What is Structural DNA Nanotechnology? This term refers to the construction of molecules with robust topological or geometrical features from DNA components. This might sound a little strange. What can we possibly make from a linear double helix, except long lines, relaxed or supercoiled circles, knots or catenanes? In fact, DNA does not need to be linear; branched molecules occur naturally in DNA metabolism, but only as ephemeral intermediates, such as the four-arm Holliday (*1*) junction or the disjoint three-arm replication fork. These intermediates are unstable, because they contain homologous sequence symmetry, allowing them to isomerize via branch migration, as shown for the Holliday junction in Figure 1a. However, now that convenient chemistry exists to prepare synthetic oligonucleotides (*2*), it is possible to eliminate this symmetry and produce DNA molecules with stable branch points, such as the stable branched junction shown in Figure 1b (*3*, *4*).

It is worth pointing out here that there may be a selective advantage to an unbranched DNA helix axis in its role as genetic material: The complement to a DNA strand is only well-defined if the complement is unbranched (*5*). For example, the left of Figure 1d shows a DNA double helix in which strand 2 complements strand 1. By contrast, the right of Figure 1d shows strand 1 complemented by a branched strand 2 molecule; the horizontal arm could be any length, and the complementarity between strands 1 and 2 would not be altered. Hence, it is not surprising that the DNA double helix is a linear molecule, linear in the sense that its helix axis is unbranched.

Sticky-ended cohesion has been used for nearly 30 years as the basis for directing the assembly of DNA molecules in genetic engineering (*6*). Sticky ends (and other cohesive interactions, e.g., ref *7*) can be combined with branched molecules to build complex graph-like target molecules; the

vertices of these molecules are the branch points of DNA branched junctions, and their edges consist of DNA double helices. Figure 1c illustrates the sticky end based self-assembly of four 4-arm junctions to make a quadrilateral; this arrangement could be extended through the sticky ends on the outside to make a 2D or 3D lattice. The affinity aspect of complementarity at DNA sticky ends is evident; binding occurs between molecules with complementary sticky ends. However, it should not be forgotten that sticky ended cohesion also results in a predictable local structure, B-DNA (*8*). Thus, sticky ended cohesion is a predictable intermolecular interaction with regard both to affinity and to structure. It is thus unique among macromolecular systems: Affinities are readily described, say, in antibody−antigen interactions, but the orientational relationship between the antibody and antigen must be established experimentally for every pair.

The Biochemical Basis of Structural DNA Nanotechnology. (a) Complementarity. Structural DNA nanotechnology is based on the common biochemical notion of structural complementarity, particularly Watson−Crick complementarity between the two strands of a DNA double helix. However, the notion requires generalization (*5*) when applied to branched molecules: It needs to be extended to include complementarity across one or more gaps, such as the gap shown in Figure 1d (right). Thus, strand 1 in Figure 1b is complementary to the group of strands 2, 3, and 4. Of course, there is traditional double helical Watson−Crick complementarity within each arm, but there is also complementarity in the sense of a four-arm junction; we will see below complementarity in the sense of a large number of different topologies, such as antijunctions and mesojunctions (*9*), double crossover (DX) molecules (*10*), or PX DNA (*11*). We will describe these unusual topologies and others below.

As noted above, stable branched junctions are produced from synthetic molecules, so there must be a method to assign sequences to them. We have been successful in using the method of sequence symmetry minimization (*3*, *12*) to design sequences. The underlying notion is that DNA strands will maximize the DNA double helical structures that they form. Although an early approach (*13*) involved calculating a likelihood of formation from nearest-neighbor equilibrium thermodynamic parameters (*14*−*16*), no constructs built to date require a calculation this extensive. The method used can be understood readily by reference to Figure 1b. This molecule contains four 16-mers, labeled 1, 2, 3, and 4. We break up each of these single strands into a series of 13 overlapping tetramers, such as the CGCA or GCAA that have been boxed; we insist that each of these be unique. In addition, we insist that each tetramer that spans a branch point, such as the boxed CTGA, not have its linear complement (TCAG) present; this restriction results in these tetramers being unable to form linear double helices. Consequently, competition with the four octamer double helical targets can occur only from trimers, such as the boxed ATG sequences.

(b) Motifs Generated by Reciprocal Exchange. Structural DNA nanotechnology originated as a natural outgrowth of attempts to model the Holliday junction recombination intermediate (*3*). Branched junctions and more complex motifs are a consequence of reciprocal exchange between two double helices. The nature of reciprocal exchange is shown in Figure 2a. A blue strand and a red strand are shown there exchanging portions to produce a blue-red strand and a red-blue strand. Although often complicated in living systems, nanotechnological systems do not actually have to undergo reciprocal exchange to produce new motifs; once the structural design process is complete, new motifs are generated directly by using the sequence assignment procedure to design strands that will self-assemble into the motif.

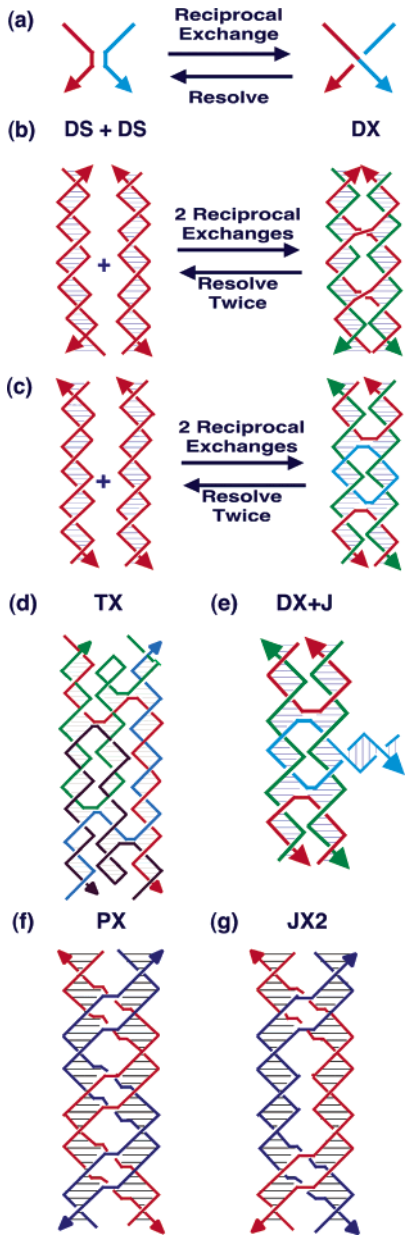

FIGURE 2: Motif generation. (a) The process of reciprocal exchange. A red strand and a blue strand exchange to form a red-blue strand and a blue-red strand. (b, c) Reciprocal exchange to form DX molecules. Two reciprocal exchanges between strands of the same polarity produce the DX molecule in panel b, and two reciprocal exchanges between strands of opposite polarity yield the (better behaved) DX molecule in (c). (d) The TX motif. This molecule results from combining the DX molecule with another double helix. (e) The DX+J motif. This molecule, usually made with the extra helix roughly perpendicular to the plane of the other two, is made by combining a DNA hairpin and a DX molecule. (f) The PX motif. This motif results from performing reciprocal exchange between two helices at all possible positions where strands of the same polarity come together. (g) The JX_2 motif. This is similar to the PX motif, except that reciprocal exchange is omitted at two adjacent juxtapositions.

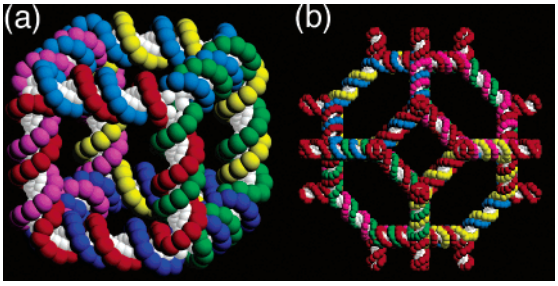

FIGURE 3: Ligated products from flexible DNA components. (a) A stick cube and (b) a stick truncated octahedron. The drawings show that each edge of the two figures contains two turns of double helical DNA. There are two turns of DNA between the vertices of each polyhedron, making them, respectively, a hexacatenane and a 14-catenane.

An example of producing a new motif by reciprocal exchange is shown in Figure 2b,c. This motif is the double crossover (DX) structure, involved in double strand break recombination (*17*, *18*) and in meiosis (*19*).

The exchange process can occur between strands of the same polarity (Figure 2b) or of the opposite polarity (Figure 2c). With a single exchange, this difference results only in conformational variation, but, as can be seen readily from Figures 2b,c, there are major topological differences when two or more crossovers are involved. The biologically relevant molecules involve crossovers between strands of the same polarity (Figure 2b). However, those molecules are not well behaved when the separation between crossovers is small (*10*). Consequently, most molecules with multiple crossovers used for nanotechnological purposes contain crossovers between strands of opposite polarity. Figure 2d,e shows two examples of these molecules, the TX molecule (*20*), containing three fused helices (similar to the DX molecule of Figure 2c) and the DX+J molecule (*21*), in which another helical domain has been added to the DX motif. Figure 2f shows the PX motif, wherein every possible exchange has been designed to occur between strands of the same polarity. A variant on this theme, the JX_2 motif (Figure 2g) has been used along with the PX motif in a DNA device (*22*).

Reciprocal exchange between double helices produces branched junctions flanked by four double helices; other numbers of helices can be produced by combining helices or junctions with hairpins (*11*). Branched junctions flanked by three (*23*), five, and six (*24*) double helices have been reported, and there is no obvious limit to the number of double helical arms that may flank a junction (*25*). This is important, because the connectivity of the graph produced by cohesion or ligation of junctions is limited by the number of arms that flank its junctions. Space-filling lattices built from the classical Platonic or Archimedean polyhedra have connectivities up to 12 (*26*).

Two polyhedral catenanes that correspond to stick figures have been prepared from branched junctions. The first of these is a DNA molecule whose helix axes are connected like the edges of a cube (*27*). As seen in Figure 3a, this molecule is a hexacatenane. Each edge contains two turns of DNA, so each face of the cube corresponds to a cyclic single strand of DNA. The red strand is on the front face, and it is linked twice to the green strand on its right, the cyan strand on the top, the magenta strand on the left, and the dark blue strand on the bottom; it is only indirectly linked to the yellow strand at the rear. The construct was built by ligation in solution; every edge contains a unique restriction site, and proof of synthesis consisted of breaking down the partial and final products to independently synthesized catenanes. The second polyhedral molecule is a truncated octahedron (Figure 3b), which is a 14-catenane, containing six strands that correspond to square faces and eight strands that correspond to hexagonal faces. This molecule, nearly 800 kD in molecular mass, was built using a solid-support methodology (*28*). Proof of synthesis was similar to that of the cube (*29*). The three- and four-arm branched junctions used for the vertices of these objects are known to be somewhat floppy, so both the level of control over synthesis and the proof of synthesis are limited to topology, rather than structure.

(c) Motifs Generated by From DNA Half-Turn Topology. The role of topology in DNA biochemistry cannot be underestimated (e.g., ref *30*). When a catenane or a knot is deposited on a surface, it will be characterized by a series of crossings or nodes, where one strand lies above another; these features are sometimes called unit tangles (*31*). Nodes may be of two enantiomeric types, as illustrated in Figure 4a. The arrangement of these nodes is characteristic of any knot or catenane. A half-turn of double helical DNA corresponds to a unit tangle in a single-stranded molecule (*32*). Thus, one can make any knot or catenane from single-stranded DNA, so long as one has a way to produce nodes of both signs. Conventional right-handed B-DNA leads to nodes that are known by convention as negative nodes, and left-handed Z-DNA (*33*) leads to positive nodes, as shown in Figure 4b. Figure 4c illustrates how this principle is used to produce the simplest knot, a trefoil knot with three nodes. The three nodes in a red knot are shown flanked by black squares. The knot strands form the diagonals of the squares, dividing them into four regions, two flanked by antiparallel strands (containing a green double-headed arrow) and two flanked by parallel strands (containing a magenta line terminating in ellipses). The strands of the DNA double helix are antiparallel, so a half-turn of DNA (about six nucleotide pairs) is shown in the antiparallel regions of the square. A trefoil knot has been built using this strategy (*34*).

In another study, a variety of topologies has been formed using a single strand that contains two separated full turns of DNA, with different propensities to form Z-DNA. Figure 4d illustrates this strand and the conditions that lead to the formation of a circle, a trefoil knot with negative nodes, a four-noded figure-eight knot and a trefoil knot with positive nodes (*35*). These four cyclic molecules are produced, respectively, by increasing ionic strength and Z-promoting conditions. A related strategy was used to produce Borromean rings from DNA (Figure 4e). Borromean rings consist of three linked circles with the characteristic that no two are linked to each other, so that cleavage of one of them results in the dissociation of the other two. This feature is brought about by a specific mixture of nodes of opposite signs. Ligation of a B-DNA three-arm junction to a Z-DNA three-arm junction results in linked rings with the Borromean property (*36*).

The relationship between topological nodes and half-turns of DNA can be used to produce new DNA motifs. In a conventional branched junction, the helix axes are pointed

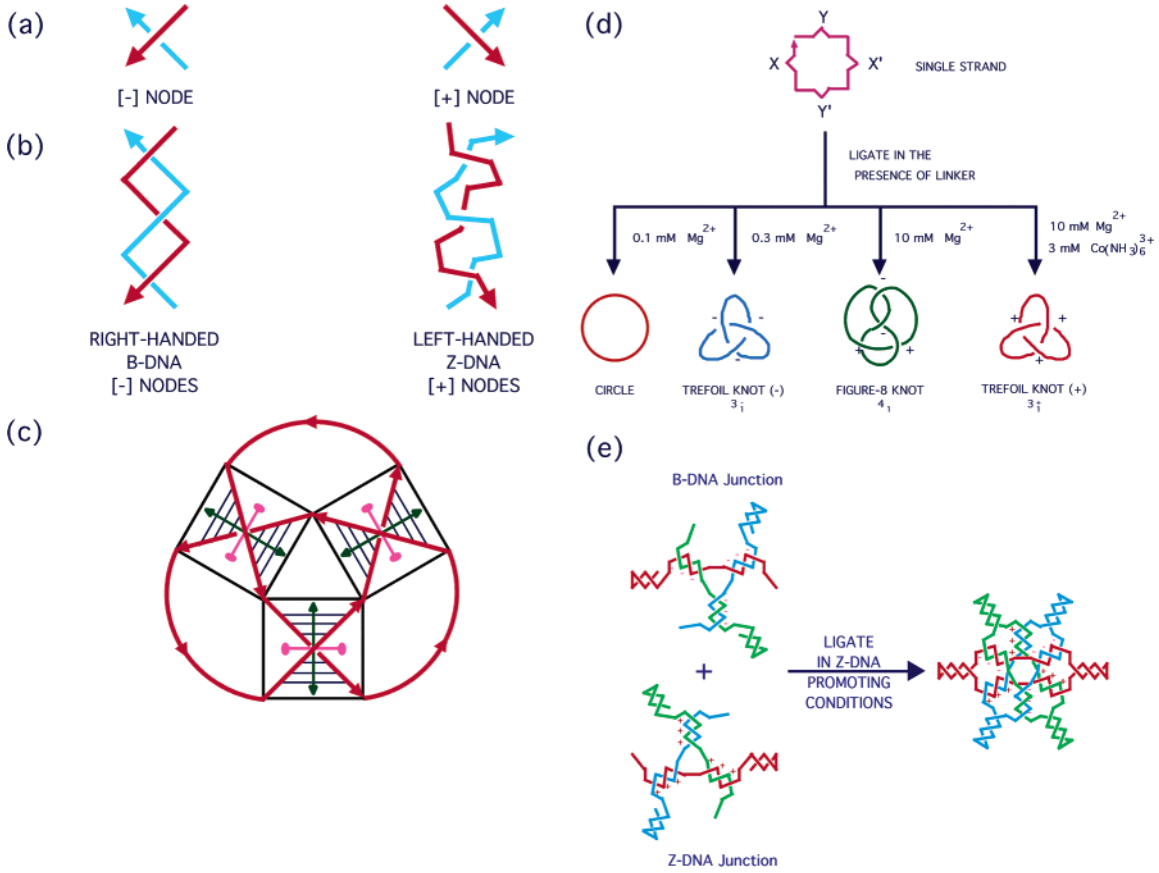

FIGURE 4: Single-stranded topology. (a) Nodes of both chiralities. The two nodes (−) and (+) are mirror images of each other. (b) Relationship of nodes to DNA. Right-handed B-DNA generates negative nodes and left-handed Z-DNA generates positive nodes. (c) DNA half-turns and knots. Three DNA half-turns are shown. They are connected with unstructured material to produce a trefoil knot. The green double headed arrows represent helix axes and the magenta lines ending in ellipses are the dyad axes of the DNA half-turns. (d) Four topologies from a single strand. The molecule contains two single-turn domains whose Z-forming propensities differ. As ionic strength is increased (left to right), the products change from a circle to a trefoil knot with negative nodes, to a figure-eight knot, to a trefoil knot with positive nodes. (e) Borromean rings from DNA. The combination of B-DNA and Z-DNA three-arm junctions produces Borromean rings.

at the center of the branch point. However, using the equivalence between nodes and DNA half-turns, it is possible to discover other relationships. Figure 5a shows a plan for the synthesis of a nine-noded knot known as 9_{49}. Every one of its nodes is flanked by stripes representing a DNA half-turn. One could imagine condensing these half-turns into larger units. For example, two-half-turns flanking a green arrow on the right could be condensed into a full-turn. Likewise, three-half-turns to the left of that position flank a red triangle, and could be condensed into a three-arm branched junction, because their helix axes point to the middle of the triangle. However, to the left of this branched junction is a grouping of four half-turns that flank an unfilled yellow square in a circumferential fashion. This arrangement is known as an "antijunction" (*9*). The filled yellow square at the top contains a combination of circumferential and centrally oriented half-turns; it is called a "mesojunction" (*9*). Figure 5b illustrates all the topologically unambiguous possibilities for three and four-strand complexes: 3_3 and 4_4 are conventional branched junctions, with all of their helix axes pointing toward the centers of their arrangements. 4_0 is the antijunction, where the dyad axes of the half-turns point toward the center of the strands and the helix axes are circumferential. 3_1, $^14_2$, and $^24_2$ are mesojunctions with mixtures of orientations. Figure 5c shows how this classification can be extended to molecules containing three-half-turns per helical domain. The antijunctions and mesojunctions are poorly behaved species, and often much experimentation is necessary to get them to form single bands on gels (*9*). Not all imaginable motifs are stable.

(d) Self-Assembly. Self-assembly of preexisting components to produce specific and functional quaternary structures is a hallmark of higher-order structure in biological systems. Viruses, microtubules, and ribosomes are but three of many cellular examples of quaternary complexes found within living systems. Structural DNA nanotechnology seeks to produce highly ordered arrangements of individual motif units. The most successful examples of self-assembly in structural DNA nanotechnology are predesigned periodic two-dimensional arrays. To produce well-structured arrays, it is necessary to use a relatively stiff motif. As noted above, individual branched junctions are somewhat flexible, so another motif is needed with more rigidity. Fortunately, the DNA double crossover (DX) molecules are stiff motifs (*21*, *37*). A combination of DX and DX+J (Figure 2e) molecules (also stiff) can be used to generate patterned arrays. DX+J molecules with their extra domains normal to the plane of the helix axes provide a topographic marker for the atomic force microscope (AFM). Figure 6a,b illustrates a pair of schematic diagrams that represent the designed patterns of two arrays. The sticky ends are represented geometrically, and the extra domain of the DX+J molecules is shown as a filled black circle. The dimensions of the tiles are about 4 × 16 nm. Consequently, one would expect to see striped

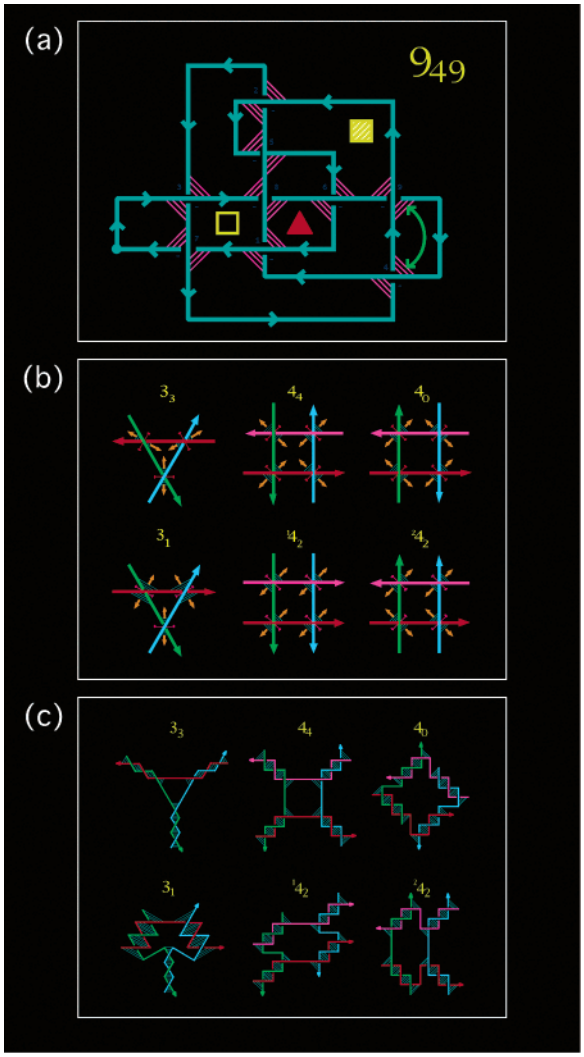

FIGURE 5: Origin and examples of antijunctions and mesojunctions. (a) A 9_{49} knot. The knot is drawn with half-turns flanking each of its nine negative nodes. These units are combined into units such as a full-turn helix (green arrow), a three-arm junction (red triangle), an antijunction (untilled yellow square) and a four-strand mesojunction (filled yellow square). (b) Half-turn representations of junctions, antijunctions and mesojunctions. Strands are drawn as thick lines, helix axes as double-headed yellow arrow, and dyad axes in magenta. 3_3 is a three-arm branched junction, 4_4 is a four-arm junction and 4_0 is a four-strand antijunction. 3_1 is a three-strand mesojunction, and $^1\!4_2$ and $^2\!4_2$ are four-strand mesojunctions. (c) Three-half-turn representations of junctions, antijunctions, and mesojunctions. The same notation applies as in panel b, but three-half-turns are involved in each helical domain.

features separated by 32 nm for the pattern in Figure 6a, and by 64 nm for the pattern in Figure 6b. The AFM images to the right of the schematics confirm these predictions (*38*).

In the same way that DX molecules can self-assemble, TX molecules can form a 2D arrangement. Figure 6c shows two TX tiles, A and B, whose first and third domains have complementary sticky ends. They form a 2D array that contains two single-helix cavities. One cavity is filled by a linear duplex molecule labeled D. Rephasing TX molecule C by three nucleotide pairs reorients it 102° to become C′. The middle domain of C′ can bind in the other cavity. This leads to helices protruding from the plane of the array in each direction. The expected pattern for this arrangement is visible in the AFM image to the right of the array (*20*).

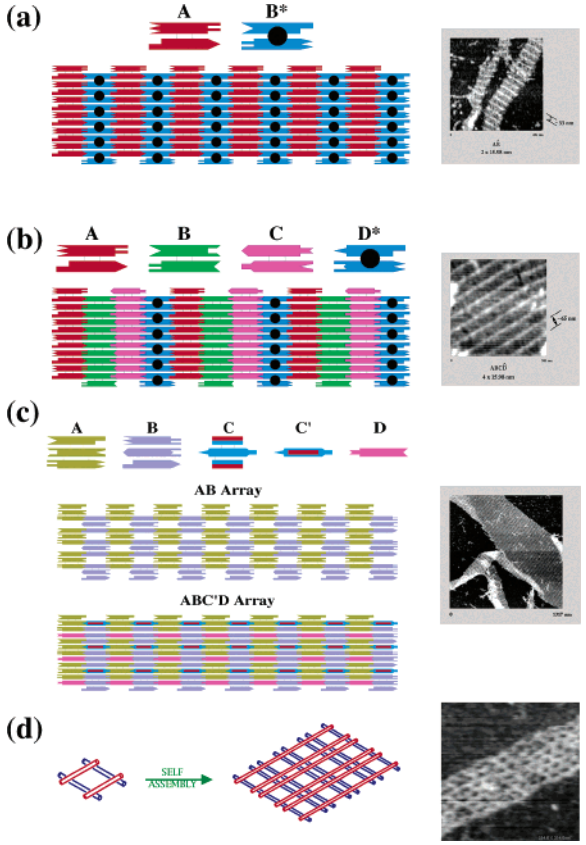

FIGURE 6: DNA Arrays. (a) Two DX molecules tile the plane. A conventional DX molecule, A, and a DX+J molecules, B*, are seen to tile the plane. The extra domain on B* leads to stripes. The molecules are 4 × 16 nm, so the stripes are ~32 nm apart, as seen in the AFM image at the right. (b) Four DX molecules tile the plane. This arrangement is similar to panel a, but there is only one DX+J molecule, D*, so the stripes are separated by ~64 nm, as seen on the right. (c) A TX Array. Two TX tiles, A and B, are connected by complementarity between their first and third double helical domains, resulting in spaces between the tiles. D is a linear duplex that fits in the yellow rows, and C is a TX rephased by three nucleotide pairs; it fits into the gray rows and extends helices beyond the AB plane in both directions, as shown in the micrograph at the right. (d) A DNA parallelogram array. Four Holliday junction analogues form a parallelogram that is extended to produce a periodic array. The sizes of the cavities in the array may be tuned. Those in the array the right are ~13 × ~20 nm.

Although the individual Holliday junction is flexible, a parallelogram made from four of them is quite robust. This parallelogram (Figure 6d) consists of two parallel edges (red) above its central plane and two other parallel edges (blue) below the plane. The plane contains the crossover points of the four Holliday junctions. A molecule with complementary pairs of sticky ends will readily form a lattice, as shown in the schematic on the left of Figure 6d. The AFM image on the right consists of parallelograms with four helical turns (~13 nm) in one direction, and six helical turns (~20 nm) in the other direction. In addition, there are two turns from large parallelogram to large parallelogram, not resolved in this AFM image (*39*).

Periodic arrangements of DNA are not the only types of self-assemblies that have been prototyped in this system. One can also program a series of DNA tiles to do computation by self-assembly. Wang tiles (*40*) are tiles with different colored edges that self-assemble into a mosaic, according to the rule that every edge in the mosaic is flanked by the

same color. It has been shown that the assembly of Wang tiles emulates the operation of a Turing machine, a general purpose computer. An example is shown in Figure 7a. Winfree (*41*) has pointed out that in principle branched DNA molecules can reduce Wang tiles to practice on the molecular scale, thus producing an algorithmic assembly. Periodicity is the simplest assembly algorithm: The tile on the left, on the right, in front, in back, above, and below are the same as the central tile, and oriented similarly; within this class are also sets of tiles (e.g., the multitile arrangements in Figures 6a−c, as well as tiles or tile groupings related to each other by space group symmetry). Physically, periodicity depends on a given tile or set of tiles creating surfaces to which further tiles can bind so as to extend the periodic lattice. The contents of a site in an algorithmic assembly are determined similarly, but, like the Wang tiles in Figure 7a, they do not lead to periodicity. Indeed, the tiles in Figure 7a correspond to a simple calculation, the addition of 5 to 9 to yield 14: Starting from the upper left, the blue-green-edged diagonal row of tiles intersects the vertical white-edged row in the fifth column. The insertion of the four-color tile at that intersection redirects the pathway horizontally along the orange-edged row until it encounters the vertical white-edged row in the ninth column. Insertion of a different four-color tile in the ninth column leads the pathway up the gray-purple-edged diagonal to the top of the 14th row. Winfree has suggested that algorithmic assemblies that "count" could be used to delimit the sizes of arrays in one or more dimensions (*42*).

The key practical difference between periodic and algorithmic assemblies is that competition for slots in periodic arrangements is between correct and incorrect tiles; by contrast, tiles in an algorithmic assembly are usually competing against partially correct tiles. Figure 7b illustrates a four-bit cumulative XOR calculation. XOR is a Boolean function whose output is 0 if the two inputs are the same and 1 if they are different. Each tile is a TX molecule containing a "reporter strand" drawn in red. The value of the tile is 0 or 1 depending on the identity of a restriction site on the reporter strand. Below that tile is a box containing schematic versions of the input X tiles (blue) and the initiator tiles (green). The tiles that perform the logic are the shown in red. The sticky ends on their bottom domains stand for 0 or 1 on the left or right ends. A self-assembly is shown below the tile box. The initiator and input tiles are held together by longer sticky ends than those holding the red tiles. Thus, in a cooling protocol, the input and initiator tiles assemble first. When this happens, a double site is created to bind the first red tile. A second double site is then created, and the process continues. In the end, the order of assembly is determined by ligating the reporter strands to form a long single strand (bottom), and then subjecting this strand to partial restriction analysis (in separate reactions for 0 and 1) to establish the values of the tiles that assembled. The error rate in this prototype problem is very low (*43*).

There are numerous types of DNA-based computation, most of which are not based on the assembly of DNA tiles. The groundbreaking experiments were originally performed by Leonard Adleman, who solved a prototype Hamiltonian path problem (related to the Traveling Salesman problem) using a series of strands that represented cities and a related set of strands that represented routes between those cities

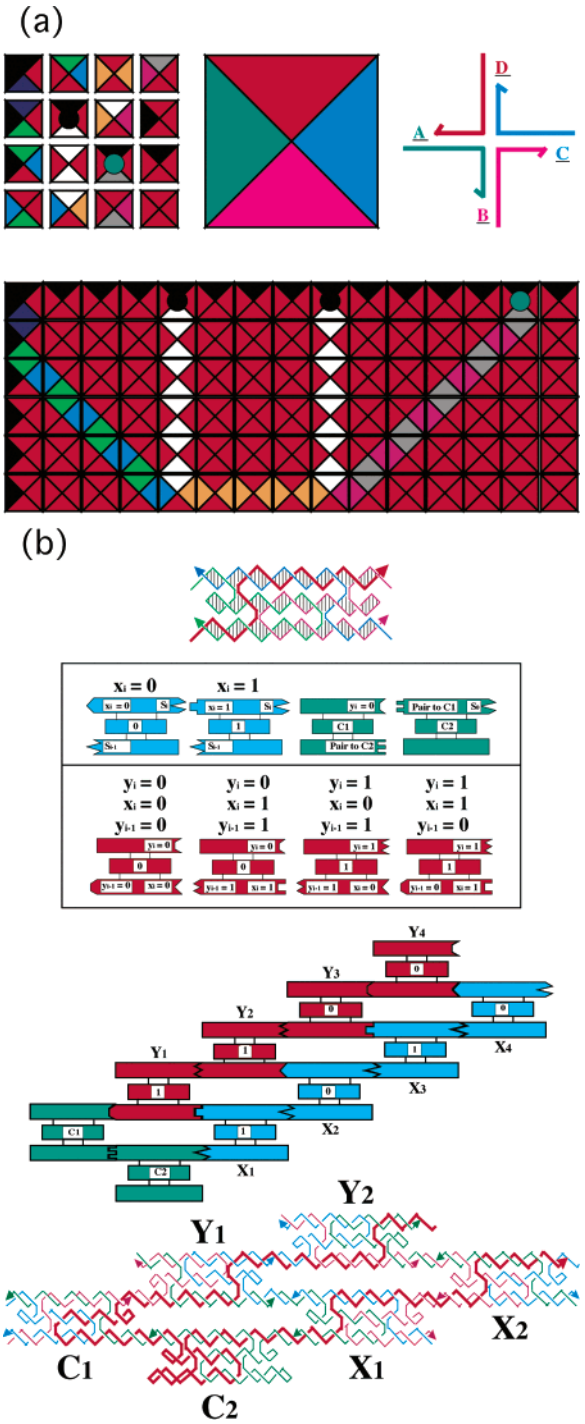

FIGURE 7: Wang tiles and algorithmic assembly. (a) Wang tiles. The upper left shows 16 wang tiles that fit together in the mosaic below according to the rule that each edge is flanked by the same color (modified from ref *40*). The relationship between Wang tiles and a branched junction with a variety of sticky ends is illustrated at the upper center and right. (b) A four-bit XOR self-assembly. At the top of the panel is a TX tiles with its reporter strand emphasized in red. Below this are schematics of the input tiles (blue), initiator tiles (green), and gating tiles (red). The four possible inputs to the XOR gate correspond to sticky ends on the bottom domains of the red tiles. The schematic tiles are shown to self-assemble to produce the output arrangement of red tiles in the schematic below this. At the bottom, the answer is extracted by ligation of the reporter strands, which are later subjected to partial restriction.

(*44*). This problem is illustrative of the types of problems best suited to DNA-based computation: Problems in which

the huge parallelism of molecular species can be used to list a large number of possible solutions, followed by a simple screen or selection for the correct answer. Of interest to biochemists is that these solutions, containing small quantities each of large numbers of different molecular species, are somewhat reflective of the situation in living cells, arguably more reflective than typical chemical systems that contain large quantities of small numbers of chemical species. Space does not allow for a description of the many types of DNA-based computation that have been reported.

DNA Transitions and DNA Nanomechanical Devices. (a) Cruciform Extrusion. One of the key goals of structural DNA nanotechnology is the design and assembly of nanomechanical devices. Three different DNA transitions have been exploited to power DNA devices. The first, rather clumsy, device, entailed the phenomenon of cruciform extrusion (*45*). Figure 8a illustrates a circle containing four mobile bases at the branch point of a cruciform. It is well-known that negative superhelical stress can cause a cruciform to be extruded from a circle, and that this stress can be relieved by the addition of an intercalating dye, such as ethidium. Thus, the addition or removal of ethidium can relocate the mobile region from the cruciform to the circle or vice versa, respectively. The use of hydroxyl radical autofootprinting (*46*) enables one to determine the position of the branch point in a mobile system, so it is relatively straightforward to demonstrate the operation of the device. The large size of the circle and the coarseness of the control suggested that a better device was needed.

(b) The B−Z Transition. As soon as it was established that the DX molecule is fairly stiff (*21*), it was possible to use that motif as the basis of a device (*47*). The driving force for the device was the B−Z transition of DNA (*33*). The formation of left-handed Z-DNA has two requirements, a sequence that is capable of undergoing the B−Z transition, and conditions that promote the transition. One can use the sequence requirement in the design of the device to control the extent of the transition in space. Likewise, the requirement for Z-promoting conditions allows one to control the timing of the transition. The device is illustrated in Figure 8b. It consists of two DX molecules joined by a shaft of linear DNA. Twenty nucleotide pairs along the shaft (colored yellow) consist of a sequence capable of undergoing the B−Z transition. While still in B-promoting conditions, those nucleotide pairs will remain in the B conformation, which leaves the two pendent helices on the same side of the shaft. The Z-promoting reagent, $Co(NH_3)_6Cl_3$, converts the yellow nucleotide pairs to Z-DNA. This causes a rotation of 3.5 turns, leaving the pendent nucleotides on opposite sides of the shaft. The change is demonstrated by fluorescence resonance energy transfer (FRET). The FRET signal derives from the pair of dyes attached to the pendent helices.

(c) Branch Migration. The B−Z device was the first robust DNA nanomechanical device, but it suffers from the fact that it is activated by a small molecule. Thus, an array of N different devices would all respond similarly, within the limits of chemical nuance (*35*), leading to two possible states, rather than 2^N structurally distinct possible states. One way to achieve specificity in addressing the devices is to make them responsive to a particular sequence of DNA. Yurke and his colleagues have developed devices with this feature (*48*). The devices utilize single-stranded branch migration,

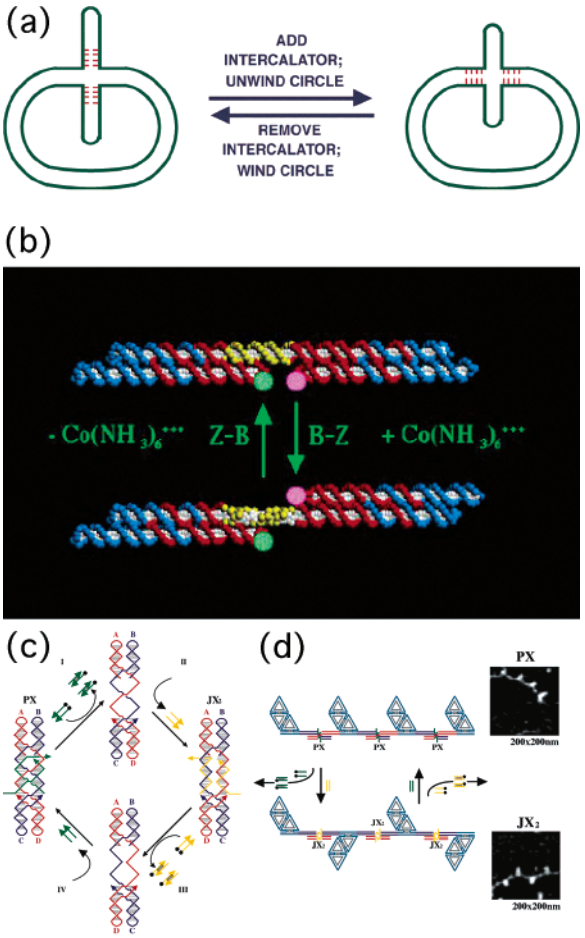

FIGURE 8: DNA devices. (a) A mobile control device. The cruciform structure on the left contains four mobile base pairs at its base. Addition of an intercalator unwinds the circle and moves them into the circle. Removal of the intercalator reverses the action of the device. (b) A DNA nanomechanical device based on the B−Z transition. The device consists of two DX molecules connected by a shaft containing 20 nucleotide pairs (yellow) capable of undergoing the B−Z transition. Under B conditions, the short domains are on the same side of the shaft, but under Z-conditions (added $Co(NH_3)_6^{3=}$) they are on opposite sides of the shaft. The pink and green FRET pair are used to monitor this change. (c) The machine cycle of a PX-JX_2 device. Starting with the PX device on the left, the green strands are removed by their complements (process I) to leave an unstructured frame. The addition of the yellow strands (process II) converts the frame to the JX_2 structure, in which the top and bottom domains are rotated a half-turn relative to their arrangement in the PX conformation. Processes III and IV reverse this process to return to the PX structure. (d) AFM demonstration of the operation of the device. A series of DNA trapezoids are connected by devices. In the PX state, the trapezoids are in a cis arrangement, but when the system is converted to the JX_2 state, they are in a trans arrangement.

to change states. We have used this principle to produce a robust rotary device using branched motifs and differential hybridization topology (*22*). The machine cycle of the device is shown in Figure 8c. It is based on the half-turn difference between the PX molecule and the JX_2 molecule (see Figure 2f,g). The molecule on the left is a PX molecule, in which the ends have been closed as hairpins; one of the red strands and one of the blue strands have been interrupted by three-half-turns of a green strand, called a “set strand”. Both of these molecules carry an extension (drawn horizontally). When the complete complement to the green set strands is added, the end binds to the extension, and then removes the

green strand through the process of branch migration (process I). The poorly structured frame, denuded of its set strands (top), is now available to bind the yellow set strands (process II), and to assume the JX_2 conformation. The state of the device can be changed back to the PX state in a similar fashion, as seen in processes III and IV. Similar principles have been used recently in devices based on the G_4 motif (*49*, *50*). The operation of the device in Figure 8c can be monitored by AFM, as shown in Figure 8d. A series of DNA half-hexagonal trapezoids is connected by the device. When the devices are in the PX state, all of the trapezoids are in a parallel arrangement. When the devices are in the JX_2 state, they are in a zigzag arrangement. This is seen in the AFM images at the right of Figure 8d.

Applications of Structural DNA Nanotechnology to Biochemistry. The contributions of structural DNA nanotechnology to biochemistry are few at this point. Nevertheless, unusual nucleic acid motifs have been used to make measurements, to demonstrate principles, and to act as substrates for enzymes. With one exception, the applications are related to characterization of the branched systems from which the basic motifs are derived. Nevertheless, the field is very young, and several projects are underway that are likely to increase the value of DNA nanotechnology on biochemistry.

(a) An RNA Knot Leads to an RNA Topoisomerase. The ability to fabricate deliberate knots from nucleic acids provided the ideal substrate to examine the issue of whether an RNA topoisomerase activity exists in nature. The interconversion of a knot and a circle of the same sequence was used to eliminate a large number of potential cleavage artifacts, because both species are closed cyclic molecules, with characteristic electrophoretic properties. Figure 9a illustrates the experimental system used to demonstrate that *Escherichia coli* topoisomerase III has RNA topoisomerase activity (*51*). The interconversion is achieved readily, although topoisomerase I does not catalyze the reaction.

(b) Symmetric Immobile Junctions. The study of branched molecules is complicated by branch migration. We have pointed out above that it is easy to block branch migration by eliminating the sequence symmetry that enables the isomerization. However, the symmetry is characteristic of recombination systems, and one would like to be able to have the symmetry present, without the migration, to characterize both energetics and enzymology. Three types of symmetric immobile junctions (SIJs) have been developed, so that the properties of branched junctions could be examined. These molecules are illustrated in Figure 9b. In the first kind of SIJ, a symmetric junction is held immobile by close coupling with an immobile junction in the context of a DX molecule (*52*). The disadvantages of this system are that the molecule is held in an unnatural conformation, directly antiparallel, and some sites are occluded from access by enzymes. Nevertheless, the system has been used to estimate quantitatively the sequence dependence of both crossover isomerization (*53*) and branch migratory isomers (*54*). In the second SIJ, a Bowtie junction containing 5′, 5′ and 3′, 3′ linkages in its crossover strands (*55*) is flanked by a symmetric sequence. The molecule is relaxed, but the strands are closer to parallel than to antiparallel, and, of course, the linkages are unnatural. This system has been used to demonstrate cooperativity between the subunits of RuvC resolvase. The

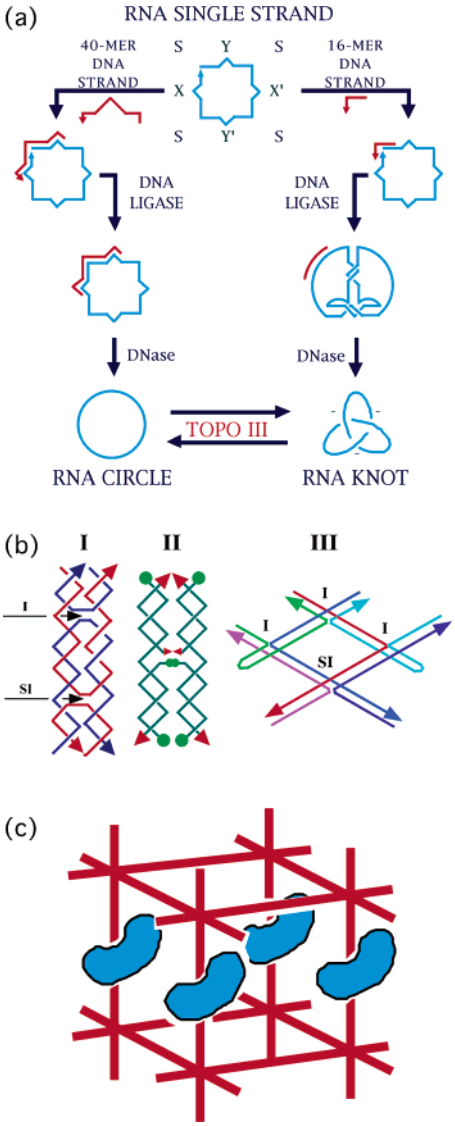

FIGURE 9: Biochemical applications. (a) Demonstration of RNA topoisomerase activity in *E. coli* topoisomerase III. The same strand of RNA forms a circle (left) or a knot (right), as a function of the length of linker used in the ligation. These species are interconverted by topo III, but not by topo I. (b) Symmetric immobile junctions. The three types of symmetric immobile junctions consist of a DX molecule with an immobile junction coupled tightly to the symmetric junction (I), a Bowtie junction, wherein branch migration is unfavorable because it would lead to parallel helices (II), and a DNA parallelogram in which an undistorted junction is held in place by close coupling to three immobile junctions in its vicinity (III). (c) A guest molecule in a DNA box. A red DNA box is drawn with sticky ends protruding from it. The idea is that such boxes could be assembled into 3D arrays amenable to diffraction analysis. The blue guests within the box would also be amenable to crystallographic analysis if they were as well ordered as the DNA host lattice.

third SIJ is based on DNA parallelograms, such as the ones shown in Figure 6d. It is immobilized in a manner similar to the first type of SIJ, but here three immobile junctions hold a symmetric junction immobile in an undistorted context. This SIJ has none of the disadvantages of the others. It has been used to demonstrate the cleavage preferences of Vaccinia topoisomerase (S. Liao, C. Mao, J. J. Birktoft, S. Shuman, and N.C.S., manuscript in preparation). In other work using type I SIJs, a DX molecule with one immobile and two symmetric junctions has been used to demonstrate

the spontaneity of branch migration in antiparallel Holliday junctions; the mobile junctions migrated after the immobile junction was restricted away (*56*). Related DX constructs (but not symmetric) have been used to demonstrate the spontaneity of crossover isomerization (*57*), the sign of the Holliday junction node (*58*) and the absence of postulated braiding in positively supercoiled molecules (*59*).

(c) Angle Measurements. Parallelogram arrays are an excellent way to measure the angle between helical domains within the Holliday junction. The junctions are unstressed, so deposition of an array on mica leads to an AFM image whose autocorrelation function provides a good estimate of the interhelical axis angle. In the immobile junction, this method yields an angle of ~63° between its helix axes, in good agreement with previous estimates. Likewise, it shows that the angle between the helix axes of the Bowtie junction is ~ −70°. This method has been applied to confirm the crystallographic determination of an unusually small angle near 40° in a symmetric sequence containing an ACC sequence (*60*). The autocorrelation function in this case indicated an angle of 43°, eliminating crystal packing forces as the cause of this unusual angle (*61*).

The Future Relationship of Structural DNA Nanotechnology to Biochemistry. There are many developments afoot in structural DNA nanotechnology that may have impact on biochemistry and molecular biology. The motivating force behind much of this program has been the notion of using 3D arrays to organize biological molecules and complexes into periodic arrays as a general method of crystallization (*3*). This idea is illustrated in Figure 9c, showing a biological macromolecule as a guest in a DNA box designed to self-assemble by sticky ends. DNA-based devices, such as those described above, may ultimately generate a nanorobotics that can be used in a variety of ways in a biological context. Other than the Holliday junction and the parallel DX molecule, there is no obvious direct relationship between any of the unusual motifs mentioned above and natural biological systems. However, the suggestion has been advanced that the PX molecule may offer a motif involved in homologous recognition in DNA molecules (*62*). It is also possible that the unusual motifs discussed above, or their congeners made of transcribed RNA, may be of use in therapeutic applications that entail nucleic acids. For example, bulky tile-like or knot-like motifs might be directed to bind to the genetic material of a virus and hamper its loading into the capsid.

The interplay of these two fields is likely to grow. Virtually all of the systems described rely on Watson−Crick base pairing. However, many new interactions has been discovered in structural studies of RNA molecules, including the ribosome. These new interactions may constitute further contributions to a tool box for nanotechnologists working with nucleic acids. For example, the recently described Tecto-RNA is a system that utilizes non-Watson−Crick interactions for intermolecular cohesion (*63*). Another key point of intersection is replication. Replication of branches is at best oblique (*64*, *65*), and suffers from topological problems. The power of nucleic acid-based nanotechnology will be increased enormously when the systems involved can be replicated in reactions catalyzed by biological polymerases. Currently, structural DNA nanotechnology is largely a biokleptic enterprise. However, it is beginning to pay back its debt to biochemistry, and the hope is that ultimately the contributions of the two fields to each other will lead to a symbiotic relationship.

ACKNOWLEDGMENT

I am grateful to all of my students, postdoctoral colleagues, and collaborators for their contributions to the founding of structural DNA nanotechnology.

REFERENCES

1. Holliday, R. (1964) *Genet. Res. 5*, 282−304.
2. Caruthers, M. H. (1985) *Science 230*, 281−285.
3. Seeman, N. C. (1982) *J. Theor. Biol. 99*, 237−247.
4. Kallenbach, N. R., Ma, R.-I., and Seeman, N. C. (1983) *Nature 305*, 829−831.
5. Seeman, N. C. (2000) *Synlett 2000*, 1536−1548.
6. Cohen, S. N., Chang, A. C. Y., Boyer, H. W., and Helling, R. B. (1973) *Proc. Natl. Acad. Sci. U.S.A. 70*, 3240−3244.
7. Zhang, X., Yan, H., Shen, Z., and Seeman, N. C. (2002) *J Am. Chem. Soc. 124*, 12940−12941.
8. Qiu, H., Dewan, J. C., and Seeman, N. C. (1997) *J. Mol. Biol. 267*, 881−898.
9. Du, S. M., Zhang, S., and Seeman, N. C. (1992) *Biochemistry 31*, 10955−10963.
10. Fu, T.-J., and Seeman, N. C. (1993) *Biochemistry 32*, 3211−3220.
11. Seeman, N. C. (2001) *Nano Lett. 1*, 22−26.
12. Seeman, N. C. (1990) *J. Biomol. Struct., Dyns 8*, 573−581.
13. Seeman, N. C., and Kallenbach, N. R. (1983) *Biophys. J. 44*, 201−209.
14. Breslauer, K. J, Frank, R., Blocker, H., and Marky, L. A. (1986) *Proc. Natl. Acad. Sci. U.S.A. 83*, 3746−3750.
15. Doktycz, M. J., Goldstein, R. F., Paner, T. M., Gallo, F. J., and Benight, A. S. (1992) *Biopolymers 32*, 349−864.
16. SantaLucia, J. (1998) *Proc. Nat. Acad. Sci. U.S.A. 95*, 1460−1465.
17. Thaler, D. S., and Stahl, F. W. (1988) *Annu. Rev. Genet. 22*, 169−197.
18. Sun, H., Treco, D., and Szostak, J. W. (1991) *Cell 64*, 1155−1161.
19. Schwacha, A., and Kleckner, N. (1995) *Cell 83*, 783−791.
20. LaBean, T., Yan, H., Kopatsch, J., Liu, F., Winfree, E., Reif, J. H., and Seeman, N. C. (2000) *J. Am. Chem. Soc. 122*, 1848−1860.
21. Li, X., Yang, X., Qi , J., and Seeman, N. C. (1996) *J. Am. Chem. Soc. 118*, 6131−6140.
22. Yan, H., Zhang, X., Shen, Z., and Seeman, N. C. (2002) *Nature 415*, 62−65.
23. Ma, R.-I., Kallenbach, N. R., Sheardy, R. D., Petrillo, M. L., and Seeman, N. C. (1986) *Nucl. Acids Res. 14*, 9745−9753.
24. Wang, Y., Mueller, J. E., Kemper, B., and Seeman, N. C. (1991) *Biochem. 30*, 5667−5674.
25. Seeman, N. C., and Kallenbach, N. R. (1988) in *Molecular Structure: Chemical Reactivity and Biological Activity* (Stezowski, J. J., Huang, J.-L. Shao, M.-C, Eds.) pp 189−194, Oxford University Press, Oxford.
26. Williams, R. (1979) *Geometrical Foundation of Natural Structure*, Dover, New York.
27. Chen, J., and Seeman, N. C. (1991) *Nature 350*, 631−633.
28. Zhang, Y., and Seeman, N. C. (1992) *J. Am. Chem. Soc. 114*, 2656−2663.
29. Zhang, Y., and Seeman, N. C. (1994) *J. Am. Chem. Soc. 116*, 1661−1669.
30. Cozzarelli, N. R., and Wang, J. C. (1990) *DNA Topology and its Biological Effects*, Cold Spring Harbor Press, New York, 11724.
31. Sumners, D. W. (1990) *Math Intelligencer 12*, 71−80.
32. Seeman, N. C. (1992) *Mol. Eng. 2*, 297−307.
33. Rich, A., Nordheim, A., and Wang, A. H.-J. (1984) *Annu. Rev. Biochem. 53*, 791−846.
34. Du, S. M., and Seeman, N. C. (1994) *Biopolymers 34*, 31−37.
35. Du, S. M., Stollar, B. D., and Seeman, N. C. (1995) *J. Am. Chem. Soc. 117*, 1194−200.
36. Mao, C., Sun, W., and Seeman, N. C. (1997) *Nature 386*, 137−138.
37. Sa-Ardyen, P., Vologodskii, A. V., and Seeman, N. C. (2003) *Biophys. J.*, in press.

38. Winfree, E., Liu, F., Wenzler, L. A., and Seeman, N. C. (1998) *Nature 394*, 539−544.
39. Mao, C., Sun, W., and Seeman, N. C. (1999) *J. Am. Chem. Soc. 121*, 5437−5443.
40. Grünbaum, B., and Shephard, G. C. (1986) *Tilings Patterns*, Freeman, New York.
41. Winfree, E. (1996) in *DNA Based Computing* (Lipton, E. J., Baum, E. B., Eds.) pp 199−219, Am. Math. Soc., Providence.
42. Winfree, E. (2000) *J. Biol. Mol. Struct., Dyns. Conversation 11-(2)*, 263−270.
43. Mao, C., LaBean, T., Reif, J. H., and Seeman, N. C. (2000) *Nature 407*, 493−496.
44. Adleman, L. (1994) *Science 266*, 1021−1024.
45. Yang, X., Vologodskii, A. V. Liu, B., Kemper, B., and Seeman, N. C. (1998) *Biopolymers 45*, 69−83.
46. Churchill, M. E. A., Tullius, T. D., Kallenbach, N. R., and Seeman, N. C. (1988) *Proc. Natl. Acad. Sci. U.S.A. 85*, 4653−4656.
47. Mao, C., Sun, W., Shen, Z., and Seeman, N. C. (1999) *Nature 397*, 144−146.
48. Yurke, B., Turberfield, A. J., Mills, A. P., Jr., Simmel, F. C., and Neumann, J. L. (2000) *Nature 406*, 605−608.
49. Li, J. J., and Tan, W. (2002) *Nano Lett. 2*, 315−318.
50. Alberti, P., and Mergny, J.-L. (2003) *Proc. Natl. Acad. Sci. U.S.A. 100*, 1569−1573.
51. Wang, H., Di Gate, R. J., and Seeman, N. C. (1996) *Proc. Natl. Acad. Sci. U.S.A. 93*, 9477−82.
52. Zhang, S., Fu, T.-J., and Seeman, N. C. (1993) *Biochemistry 32*, 8062−8067.
53. Zhang, S., and Seeman, N. C. (1994) *J. Mol. Biol. 238*, 658−668.
54. Sun, W., Mao, C., Liu, F., and Seeman, N. C. (1998) *J. Mol. Biol. 282*, 59−70.
55. Sha, R., Liu, F., Iwasaki, H., and Seeman, N. C. (2002) *Biochemistry 41*, 10985−10993.
56. Sha, R., Liu, F., and Seeman, N. C. (2000) *Biochemistry 39*, 11514−11522.
57. Li, X., Wang, H., and Seeman, N. C. (1997) *Biochemistry 36*, 4240−4247.
58. Fu, T.-J., Tse-Dinh, Y.-C., and Seeman, N. C. (1994) *J. Mol. Biol. 236*, 91−105.
59. Sun, W., Mao, H., Iwasaki, H., Kemper, B., and Seeman, N. C. (1999) *J. Mol. Biol. 294*, 683−699.
60. Eichman, B. F., Vargason, J. M., Mooers, B. H. M., and Ho, P. S. (2000) *Proc. Natl. Acad. Sci. U.S.A. 97*, 3971−3976.
61. Sha, R., Liu, F., and Seeman, N. C. (2002) *Biochemistry 41*, 5950−5955.
62. Shen, Z. (1999), Ph.D. Thesis, New York University.
63. Jaeger, L, Westhof, E., and Leontis, N. B. (2001) *Nucl. Acids Res. 29*, 455−463.
64. Seeman, N. C. (1991) *DNA Cell Biol. 10*, 475−486.
65. Eckardt, H. E., Naumann, K., Pankau, W. M., Rein, M., Schweitzer, M., Windhab, N., and von Kiedrowski, G. (2002) *Nature 420*, 286−286.

BI030079V